Comparing Low-Cost DIY and Research-Grade Hyperspectral Imaging as Coral Reef Monitoring Tools

Conor A. Hendrickson *, Peter Butcherine, Daniel P. Harrison, Brendan P. Kelaher

Posted Date: 5 May 2026

doi: 10.20944/preprints202605.0114.v1

Keywords: hyperspectral imaging; low cost; coral; bleaching; marine heatwaves

 doi:10.20944/preprints202605.0114.v1

Article

Comparing Low-Cost DIY and Research-Grade Hyperspectral Imaging as Coral Reef Monitoring Tools

Conor A. Hendrickson *, Peter Butcherine, Daniel P. Harrison and Brendan P. Kelaher

National Marine Science Centre, Southern Cross University. 2 Bay Drive, Coffs Harbour NSW 2450
* Correspondence: c.hendrickson.11@student.scu.edu.au

Highlights

- A low-cost (~USD $200) open-source HSI device was compared against a research-grade (~USD $70,000) commercial hyperspectral camera and found to measure similar spectral responses in reference lights and coral photosynthetic pigments.
- The low-cost HSI was unable to resolve differences in spectral magnitude as accurately as the commercial HSI.
- The current design is better suited to classification and diagnostic applications rather than quantifying bleaching severity.
- Continued development of affordable HSI platforms benefits coral research and environmental monitoring more broadly

Abstract

Hyperspectral imaging (HSI) is emerging as a promising tool in scientific endeavours, including non-invasive quantification of pigments, an area of research with many use cases. Here, we tested the efficacy of a low-cost (~USD $200) and open-source HSI device (400 – 1000 nm, a spectral resolution of ~2 nm FWHM) in coral bleaching research. Specifically, we evaluated its ability to quantify the concentration of key photosynthetic pigments (chlorophyll *a*, chlorophyll *c*2, diadinoxanthin, peridinin, and total pigment content) was compared against a research-grade (~USD $70,000) commercial hyperspectral camera using coral fragments subjected to varying levels of thermal stress. The low-cost HSI acquired coral reflectance spectra that were similar to the commercial hyperspectral camera, with a mean spectral angle of 11.38 ± 3.82°. However, the low-cost device was unable to resolve differences in spectral magnitude to the same accuracy as the commercial HSI and did not detect differences among coral fragments at different levels of thermal stress. Thus, the current HSI device prototype is better suited for classification and diagnostic applications where spectral shape is of greater importance than spectral magnitude. Partial Least Squares Regression models built from the reflectance spectra of each HSI instrument showed very similar yet moderate performance when predicting key coral pigments (Commercial HSI mean %RMSEP = 22.8%, low-cost HSI = 22.12%). While the current design of the low-cost HSI device has clear limitations, the results show potential in a system that costs a fraction of commercial alternatives. Continued development of low-cost HSI platforms is accelerating rapidly across a variety of fields in environmental research, and improved designs have the potential to enhance coral reef monitoring and restoration efforts globally.

Keywords: hyperspectral imaging; low cost; coral; bleaching; marine heatwaves

 doi:10.20944/preprints202605.0114.v1

Introduction

Hyperspectral imaging (HSI) is a remote sensing technology used for a wide variety of applications (Cheng et al., 2025). Hyperspectral imaging is differentiated from multispectral imaging (MSI) by a larger number of bands, with hyperspectral cameras typically described as being able to collect a near continuous range of several hundred equally spaced wavebands with narrow Full Width at Half Maximum (FWHM), while MSI sensors measure fewer (typically <15) wider wavebands (Polder & Gowen, 2021). The ability of hyperspectral cameras to capture non-invasive quantitative data makes them a powerful tool for ecological monitoring. Hyperspectral images contain two spatial dimensions (x and y pixel position) and one spectral dimension (λ). The image acquisition method and characteristics of the spectral dimension can vary greatly depending on the design of the imaging system. The four main imaging systems are whiskbroom, pushbroom, band sequential spectral scanners, and snapshot cameras (Bhargava et al., 2024), with each system differing in how the three dimensions of the image are captured (Figure 1). Additionally, HSI systems vary in the spectral regions they image, from ultraviolet (UV, 100 – 400 nm) to the visible spectrum (400 – 700 nm), to near-infrared (NIR, 700–1100 nm) and beyond into the infrared and thermal-infrared ranges.

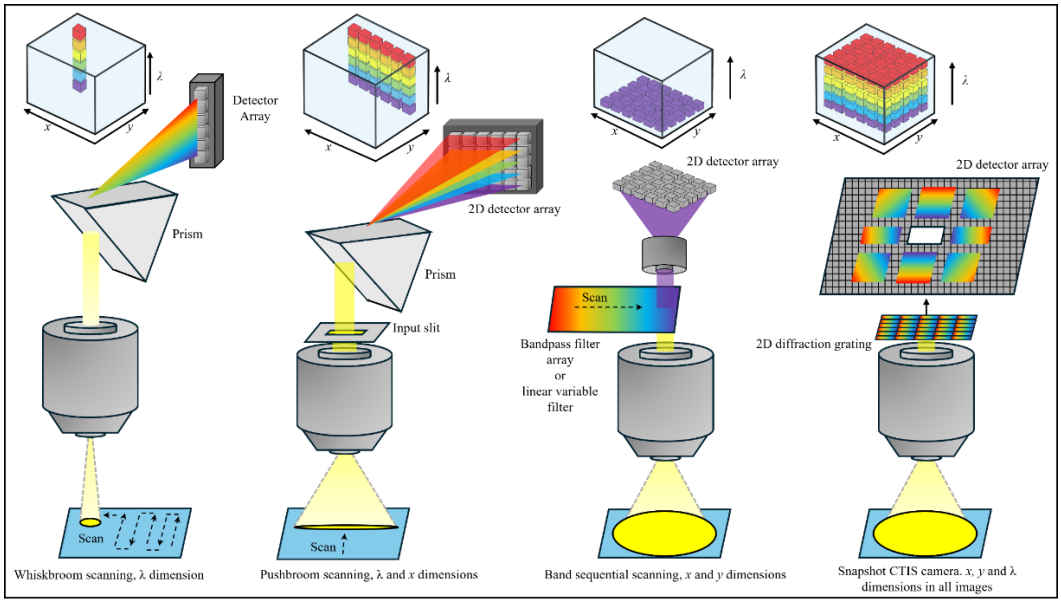

Figure 1. Common configurations of Hyperspectral imagers (HSIs) and their methods of separating x, y and λ (wavelength) dimensional data and constructing hypercubes (CTIS: Computed tomography imaging spectrometer).

Several hyperspectral camera systems have been developed for classification and mapping of underwater habitats or predicting biological characteristics such as pigment concentration including the "HyperDiver" camera by Chennu et al. (2017) and Rashid & Chennu (2020), as well as the Bi-frost DSLR by Teague et al. (2022) (Reviewed by Montes-Herrera et al., 2021). Using HSI as a bio-optical tool to assess coral reefs is of particular interest, as quantifying the concentration of photosynthetic pigments within the coral's photosynthetic algal symbionts is an essential part of assessing the health of corals. However, current methods of quantifying coral pigment concentrations require the collection of coral tissue in a destructive/invasive process. Previous studies have demonstrated that the reflectance spectrum can be used to distinguished between bleached and healthy coral (Holden & LeDrew, 1998). Also, the reflectance spectrum of coral can be used to predict the concentration of a variety of pigments (Hochberg et al., 2025) with the reflectance of coral near ~574 nm, 608 nm and 676 nm being associated with peridinin, diadinoxanthin and chlorophyll *a* pigments respectively (Teague et al., 2022). Wider implementation of HSI techniques to estimate pigment content for coral research has been limited due to the many complexities of hyperspectral imaging, including variation in spectral signals among species (Hochberg et al., 2004). This unique "optical fingerprint" results in varying magnitudes of spectral response among species, necessitating

 doi:10.20944/preprints202605.0114.v1

the prior characterisation of the species' spectral signature before the data can be used for bleaching quantification (Rashid & Chennu, 2020; Zeng et al., 2022).

Nonetheless, the largest barrier to HSI-based research has been the high costs of the systems, generally starting at USD ~$14,000 for just the instrument, without software or lighting arrays. A number of low-cost, open-source HSI devices have been created (Abd-Elrahman et al., 2011; Stuart et al., 2021; Teague et al., 2021; L. Wang et al., 2020), but their accuracy can vary widely due to the variety of optical designs and calibration methods used. In addition, there is great variation in the cost (~USD $70 to 7,000), parts acquisition, and difficulty of assembly of these systems. In this experiment, a snapshot-style, computed tomography imaging spectrometer (CTIS) hyperspectral camera designed by Salazar-Vazquez & Mendez-Vazquez (2020) was identified as one of the lowest-cost and simplest to build open-source HSI designs using commercially available components. Here, the snapshot HSI was built, calibrated, and utilised in a coral bleaching experiment to test hypotheses about the performance of the low-cost HSI compared to a high-end commercial hyperspectral camera using laboratory assayed pigment concentration from the same coral samples at different timepoints and bleaching severities.

Methods

Collection and Acclimation of Coral

This experiment was conducted at the National Sea Simulator, Australian Institute of Marine Science, Townsville. The measurements for the present study took place during the experiment described in Butcherine et al. (2026) where further details on coral husbandry, acclimation, water quality and other environmental parameters are detailed.

On February 23, 2023 ten colonies of *Acropora kenti* were collected from Davies Reef (-18° 49' 3.396", 147° 38' 45.050") near Townsville, Australia. The colonies were collected at depths of four to six metres and at a distance from one another to minimise the chance of colonies being genetically identical. The colonies were held for three days post-collection and then fragmented into 3 – 5 cm long nubbins. The fragmented corals were randomly distributed amongst the experimental tanks, but with a balanced number of fragments from each colony to reduce the potential for genotypic effects. The fragments were held for 55 days to acclimate to the 12 × 50 L experimental tanks prior to the start of the experiment. Each tank was supplied with 0.2 µm filtered flow-through seawater at a rate of 0.8 L min^{-1}. During acclimation, seawater temperature was maintained at 28.4 °C. Temperature was measured at 5 min intervals using the SeaSim proprietary datalogging system and Ds18b20 probes (n = 7). Circulation pumps provided water movement within the tanks at a rate of 1800 L h^{-1}. Artificial lighting in a 12 h light:dark photoperiod was provided by custom lights developed at the Australian Institute of Marine Science (Seasim 2g). The fragments were fed daily with a mix of instar I *Artemia salina* at a rate of 0.5 nauplii mL^{-1} and microalgae enriched rotifers at a rate of 0.35 ind. mL^{-1}.

Experimental Design

A 65-day bleaching summer was simulated with the seawater temperature manipulated as an orthogonal experimental factor with three levels: no heat-stress (control; 0 °C-weeks), moderate heat-stress (4 °C-weeks) and high heat-stress (6 °C-weeks) and one nested factor of tank, with four replicate 50 L tanks per temperature level (12 tanks in total). The intensity of the artificial lighting and the maximum monthly mean of 28.5 °C were determined using data collected *in-situ* at Davies Reef at a depth of 5 m. Two doldrum periods of heightened thermal and light-stress (Richards et al., 2024) were simulated with ramp-up and down periods (Supplementary Figure S1). Coral tissue samples and hyperspectral images were taken over three sampling events (Days 39, 52 and 65). Three coral fragments were randomly selected from each tank for each sampling event and imaged with the low-cost hyperspectral camera and high-end commercial camera prior to tissue removal.

 doi:10.20944/preprints202605.0114.v1

Coral-ACTIS

The low-cost HSI device, henceforth referred to as the Coral-ACTIS (Coral – accessible computed tomography imaging spectrometer) was based on the design proposed by Salazar-Vazquez & Mendez-Vazquez (2020) and uses a CTIS optical design to acquire spectral images (116 × 110 pixels) with a spectral resolution of (~2 nm; 315 wavebands; 400 – 1052 nm; Figure 2). The Coral-ACTIS used a portable Linux-based appimage "SquareHSI V1" Salazar-Vazquez & Mendez-Vazquez (2020) and commercially available parts including a Sony 8 megapixel IMX219 image sensor mounted on a Raspberry PI NOIR V2 module housed in a small 3d printed enclosure. The total cost of the device and required calibration lights was USD $201 (USD ~$225 if a 3d printing service is required).

For the low-cost HSI device, light is first focused by the primary lens before passing through a square aperture to reduce light scattering within the camera. The image is magnified by a macro lens before passing through a diffraction grating, which disperses the light into spatially separated diffraction orders, which are then detected by the camera sensor. The image detected by the camera sensor consists of the zero-order diffraction, which is used only for spatial identification. In the first-order diffraction, pixel position corresponds to wavelength, and pixel intensity corresponds to the reflectance of each pixel within the field of view (Figure 2).

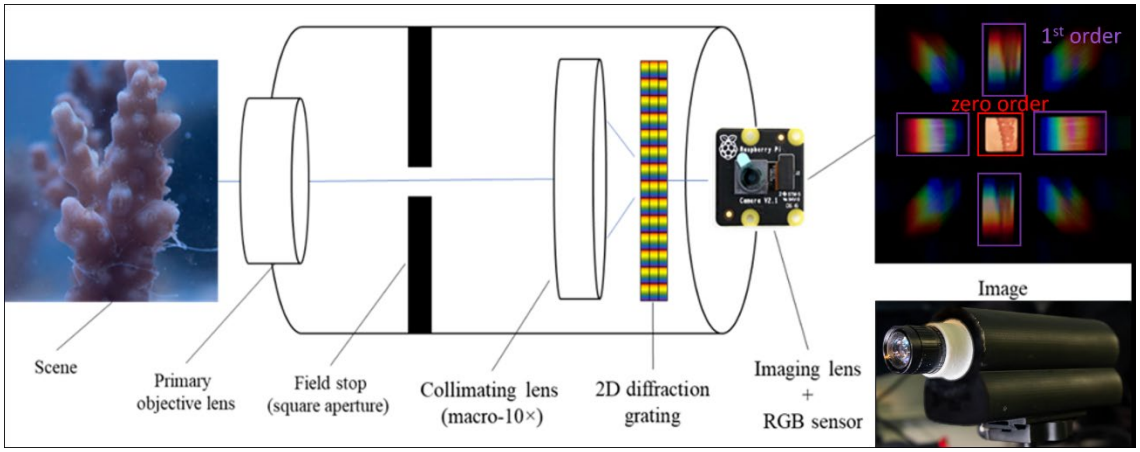

Figure 2. Coral-ACTIS (accessible computed tomography imaging spectrometer) based on the design proposed by Salazar-Vazquez & Mendez-Vazquez (2020).

Images of coral fragments were taken concurrently using the low-cost Coral-ACTIS and Resonon Pika XC2 hyperspectral camera (see description below) under the Resonon halogen bulb lighting array. An Ocean Optics Flame Series Miniature Spectrometer acquired spectra from a Compact Fluorescent Lamp (Olsent CFL Spiral ES 23W 4100K) and a Halogen bulb (Lucci Halolux 111950 42w 2700K) for use in the calibration and evaluation of the Coral-ACTIS's spectral response. The camera can also be calibrated without a costly high-resolution spectrometer if the CFL spectra are published by the bulb manufacturer (Salazar-Vazquez & Mendez-Vazquez, 2020). The images taken using the Coral-ACTIS were calibrated and processed using the Linux "SquareHSI" app provided by Salazar-Vazquez & Mendez-Vazquez (2020). A custom R script was developed to select regions of interest (ROIs) within the images for analysis and extract the relevant spectral data from the 3d hypercube files (x, y and λ). To enable comparison with the Commercial HSI, the Coral-ACTIS spectra were scaled (0–100%) using dark-noise corrections and a Spectralon 99% reflectance standard.

Commercial HSI

The Resonon Pika XC2 pushbroom HSI is a research-grade (~USD $70,000for camera, with linear translation stage and lighting array) hyperspectral camera. The Pika XC2 features a wavelength range of 390 – 1000 nm, 1600 spatial pixels and 447 channels with a Full Width at Half Maximum (FWHM) of 1.9 nm. The Pika XC2 was fitted with a Schneider Kreuznach Cinegon 6 mm f/2.1 lens and fitted into a linear translation stage with a custom Resonon lighting array (4 × Solux MR16 4700 K).

 doi:10.20944/preprints202605.0114.v1

Spectronon v3.4.7 was used to convert the raw digital numbers from the hyperspectral image datacubes into radiance (microflicks) using a radiometric calibration pack. The radiance units were then converted into reflectance (0–100%) using a Spectralon 99% reflectivity standard and dark noise measurements. ROIs were selected using the selection tools in the Spectronon software. The Savitzky–Golay algorithm was used to smooth the spectra, reduce high-frequency instrument noise, and retain spectral features in both the Resonon Pika XC2 and Coral-ACTIS spectra (window size = 9, polynomial order = 3, derivative order = 0; Savitzky & Golay, 1964).

Coral Pigment Analysis

The details of the coral tissue removal, homogenisation, centrifugation and pigment extraction are detailed in Butcherine et al. (2026). Following extraction, 250 µl of sample supernatant was added in duplicate to polypropylene microplates for spectral analysis from 400 to 700 nm in 2 nm steps using a Synergy H4 hybrid multi-mode microplate reader. The spectra were then blank and path-length corrected and the resulting spectra deconvoluted to obtain concentrations of individual pigments (chlorophyll *a*, chlorophyll *c*2, diadinoxanthin and peridinin) following (Thrane et al., 2015). Beta-carotene was also detected but accounted for less than 3% of total pigments in all treatments and was not analysed. Both symbiont density and pigment content were normalised to fragment surface-area obtained via the single-wax dipping method (Veal et al., 2010).

Statistical Analysis

Spectra of CFL and halogen light bulbs acquired with the Coral-ACTIS were compared with reference spectral measurements obtained with an Ocean Optics Flame Series Miniature Spectrometer. The association of the two spectra was assessed using Pearson correlation and Spectral Angle Mapping (SAM) of the scaled spectra, computed using the standard SAM formula (Kruse et al., 1993). SAM compares spectral signal shape by calculating the angle between the Coral-ACTIS pixel values and a reference spectrum in an n-dimensional space where n equals the number of wavelength bands. Angles approaching 0 radians (0°) indicate near-identical spectral shape, while angles approaching 1.5708 radians (90°) have near-zero shared variance. SAM was also used to compare the spectra of coral replicates acquired with each HSI by calculating the spectral angle between the paired Coral-ACTIS and Resonon Pika XC2 spectra for each coral replicate. To simplify analysis and comparison of coral spectra, the wavelength range of each instrument was limited to 500 – 700 nm for all analyses, as this range contained all spectral features relevant to the key coral pigments in *Acropora kenti*, which was the species tested.

Primer v. 7 + (PRIMERe Pty. Ltd) was used to perform Permutational analysis of variance (PERMANOVAs) based on Euclidean distance dissimilarity matrices and 9999 unrestricted permutations (Anderson, 2001). PERMANOVAs were used to determine if the bleaching severity across treatments and sampling days are interpreted differently when measured with HSI. The final PERMANOVA model had three factors: sampling day (3 levels: Day 39, 52, and 65), temperature treatment (3 levels: control, moderate heat-stress, and high heat-stress), tank as a random factor nested within temperature and all interactions. Significant tank effects were detected within the random tank factor but were not explored further as differences among tanks were not relevant to the comparison of the hyperspectral cameras. Colony was initially included as a factor in the models, but was removed when no significant main effects or interactions were found.

Partial least squares regression (PLSR) was used to quantify relationships between the Resonon and Coral-ACTIS reflectance predictors and the lab-assayed response variables and to compare predictions of pigment concentration. PLSR reduces collinear predictor variables into a smaller set of latent variables while preserving relationships between the predictor and response variables (Carrascal et al., 2009). The PLSR analysis was completed following Burnett et al. (2021) using the R Package "pls" (Mevik & Wehrens, 2007). The lab-assayed response variables were tested for homoscedasticity and normality, and in all cases, a cube-root transformation was used to reduce positive skew and conform to normality. The hyperspectral reflectance data from both the Commercial HSI and the Coral-ACTIS were not transformed as recommended by Burnett et al. (2021).

 doi:10.20944/preprints202605.0114.v1

The dataset was partitioned into calibration (80%) and validation (20%) sets, stratified by sampling event to ensure balanced representation across events. The optimal number of components (NoC) was determined by performing 50 jackknife iterations within the calibration set, each time randomly splitting the calibration data into a 70% training and 30% test subset, fitting the PLSR model up to 20 components, and calculating the predicted residual error sum of squares (PRESS) statistic for each NoC. The partitions were stratified by sampling day to avoid unbalanced partitions. The NoC with the minimum mean PRESS was selected for each pigment and HSI reflectance pair.

After determining the optimal NoCs the data was split into 80% calibration and 20% validation sets 50 times, each time the relative root mean square error of prediction (%RMSEP) was calculated. This was done to determine how different splits of the data into calibration and validation sets affected the model's reliability and predictive performance. Out of the 50 splits, the one with the closest %RMSEP to the mean was selected as the most representative and used as the final model. Using the optimal NoCs, the representative data split was then bootstrap resampled 80 times, each time leaving out one sample from the validation set to produce slightly different predicted values. The 95% prediction intervals for each HSI were then calculated based on the spread of the predicted concentration of each pigment across the resamples. The variable influence on projection (VIP) for each HSI and pigment concentration was used to evaluate the importance of each wavelength in the prediction of tissue concentration. Key wavelengths (542, 560, 676 and 694 nm) as well as important 10 nm averaged (538 – 546 nm, 556 – 564 nm, 690 – 698 nm) and 50 nm averaged reflectance regions (510 – 560 nm, 570 – 620 nm and 650–700 nm) were identified using the results of the VIP analysis and other studies of coral reflectance and pigment content (Hochberg et al., 2025; Teague et al., 2022). The 10 nm and 50 nm bands were chosen to evaluate the effects of spectral resolution to determine if lower resolutions were less effective at detecting changes.

Results

Comparing Coral Reflectance Between Instruments

The coral reflectance spectra were comparable in shape between instruments (Figure 3). The pigment absorption peak from 580 to 600 nm was visible in the Coral-ACTIS signal and aligns well with the Resonon spectra. However, the larger chlorophyll absorption peak and reflectance drop centred around 680 nm was absent, with a more gently downwards slope in the Coral-ACTIS signal, especially on Day 39. The Coral-ACTIS was able to identify some differences in reflectance among heat-stress treatments with lower reflectance and increased pigmentation in the control groups. However, PERMANOVAs tests of reflectance at key wavelengths (542, 560, 676 and 694 nm) ,as well as important 10 nm wide (538 – 548 nm, 556 – 566 nm, 690 – 700 nm) and 50 nm wide reflectance regions (510 – 560 nm, 570– 620 nm, 650–700 nm), showed that these differences were not significant when measured using the Coral-ACTIS, while the same wavelengths were significantly different among temperature treatments when measured with the Resonon Pika XC2 (Control = Moderate heat-stress, High heat-stress > Control and Moderate heat-stress treatments, Table 1; Supplementary Table S2).

Table 1. Summary of PERMANOVA main effect results.

Instrument.	Reflectance variable	Day		Temp		Day×Temp		Tank		Day×Tank	
		F	*P*	*F*	*P*	*F*	*P*	*F*	*P*	*F*	*P*
Resonon Pika XC2	542 nm	11.0930	**0.0004**	6.6131	**0.0139**	1.2761	0.3276	2.0603	**0.0459**	1.1048	0.3602
	560 nm	15.2380	**0.0003**	7.5320	**0.0133**	1.5524	0.2269	1.9872	0.0518	0.9901	0.4765
	676 nm	8.9971	**0.0023**	7.0610	**0.0111**	0.9586	0.4504	2.1819	0.0331	1.6281	0.0836

 doi:10.20944/preprints202605.0114.v1

	694 nm	27.4860	**0.0001**	8.1869	**0.0135**	1.5657	0.2302	2.7707	**0.0091**	1.4286	0.1543
	10 nm waveband (538 – nm)	54611.1160	**0.0008**	6.6158	**0.0138**	1.2775	0.3164	2.0606	**0.0450**	1.1039	0.3604
	10 nm waveband (556 – nm)	56415.2780	**0.0003**	7.5442	**0.0130**	1.5526	0.2358	1.9844	0.0511	0.9889	0.4734
	10 nm waveband (690 – nm)	69827.3690	**0.0001**	8.0708	**0.0108**	1.5482	0.2281	2.7627	**0.0098**	1.4495	0.1477
	50 nm waveband (510 – nm)	56010.7760	**0.0012**	6.4498	**0.0176**	2.0762	0.0568	6.4498	**0.0176**	6.4498	0.0176
	50 nm waveband (570 – nm)	62021.7020	**0.0001**	21.7020	**0.0001**	1.7757	0.1869	1.9818	**0.0533**	0.9286	0.5348
	50 nm waveband (650 – nm)	70013.9740	**0.0004**	7.5606	**0.0108**	1.0656	0.4098	7.5606	**0.0108**	1.0656	0.4098
Coral-ACTIS	542 nm	48.2960	**0.0001**	2.3631	0.1611	1.2583	0.3287	1.8690	0.0698	1.1959	0.2933
	560 nm	46.6430	**0.0001**	2.3087	0.1579	0.8950	0.4917	2.0313	0.0516	1.4634	0.1432
	676 nm	46.4310	**0.0001**	2.8527	0.1240	4.5216	0.1370	1.4033	0.2056	0.3838	0.9848
	694 nm	13.9790	**0.0002**	0.3620	0.7100	0.8974	0.4975	1.8476	0.0757	0.7115	0.7784
	10 nm waveband (538 – nm)	54848.4130	**0.0001**	2.3646	0.1586	1.2543	0.3281	1.8785	0.0727	1.2026	0.2909
	10 nm waveband (556 – nm)	56646.9930	**0.0001**	2.3160	0.1636	0.8948	0.4876	2.0334	**0.0483**	1.4627	0.1420
	10 nm waveband (690 – nm)	70014.9610	**0.0004**	0.3756	0.7003	0.9202	0.4741	1.8622	0.0746	0.7007	0.7826
	50 nm waveband (510 – nm)	56055.7290	**0.0001**	2.4832	0.1486	1.2832	0.3195	2.1078	**0.0415**	1.2546	0.2503
	50 nm waveband (570 – nm)	62089.4000	**0.0001**	2.9411	0.1324	0.8197	0.5181	1.9763	**0.0563**	1.2258	0.2765
	50 nm waveband (650 – nm)	70064.0800	**0.0001**	2.0895	0.1928	4.1928	0.2030	1.6090	**0.1288**	0.3642	0.9878

 doi:10.20944/preprints202605.0114.v1

Coral-ACTIS vs Resonon	Spectral similarity (SAM)	9.7210	**0.0019**	3.0434	0.0911	0.7595	0.5624	1.6382	0.1206	1.3143	0.2141

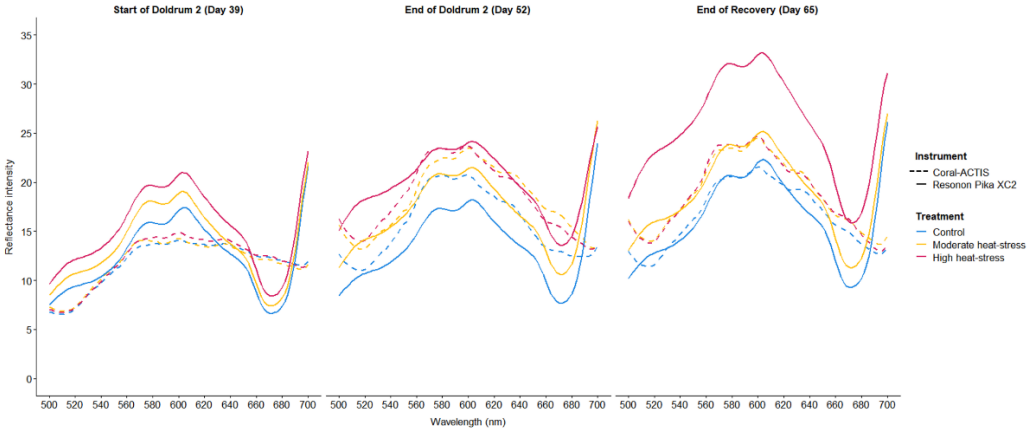

Figure 3. Comparison of mean reflectance intensity (0–100%) of *Acropora kenti* coral fragments obtained using Coral-ACTIS (dashed lines) and Resonon Pika XC2 hyperspectral camera (solid lines). Resonon reflectance intensity is radiometrically calibrated while the Coral-ACTIS uses digital numbers based on the 0–255 8-bit RGB scale. Both instruments were scaled using dark noise corrections as zero and a Spectralon 99% reflectance standard as 100%.

The Coral-ACTIS and Resonon commercial HSI both detected significant differences in reflectance at key wavelengths as a result of sampling day (Table 1). Pairwise tests for sampling day were largely similar between the two instruments, but the Coral-ACTIS did not find significantly higher reflectance at 560 or 694 nm on Day 52 compared to Day 65 where the Resonon did. For each instrument, the reflectance at individual (2 nm), 10 nm and 50 nm wide wavebands was compared but PERMANOVA results remained consistent regardless of waveband width (Supplementary Table S1).

Spectral angle mapping analysis showed a mean angle of 0.199 ± 0.067 radians (11.38 ± 3.82°) across all treatments and sampling days. PERMANOVA analysis of spectral angles showed significantly higher angles (less similarity) on Day 39 compared to the other sampling days (Figure 4; Table 1). Spectral similarity between the Coral-ACTIS and Commercial HSI was not significantly affected by treatment or tank effects (Figure 4; Table 1).

 doi:10.20944/preprints202605.0114.v1

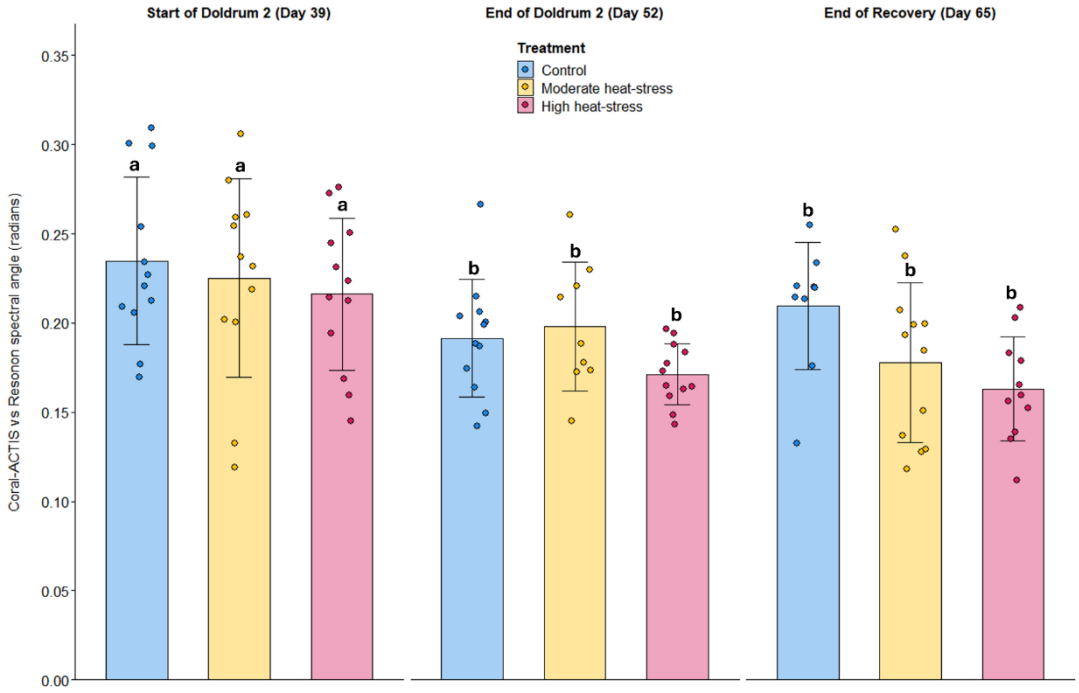

Figure 4. Coral-ACTIS vs Resonon Pika XC2 spectral angle values (0–90°) ± SD for *Acropora kenti* coral fragments across sampling days and temperature treatments. Lower spectral angles indicate higher similarity to the Resonon reference spectra shape. Letters above bars denote significant differences based on PERMANOVA results.

Predicting Coral Pigment Concentration

Partial Least Squares Regression results showed that the two HSIs were largely comparable in their prediction of key pigments, but both were only moderate predictors (Figure 5). The best predicted coral pigment was the total concentration of all pigments (Resonon %RMSEP = 17.7%, Coral-ACTIS = 20.8%), while diadinoxanthin had the highest prediction error (Resonon %RMSEP = 29.5%, Coral-ACTIS = 21.2%). The %RMSEP values were largely similar for each HSI (Resonon mean %RMSEP = 22.8% ± 4.27%; Coral-ACTIS = 22.12% ± 1.89%), with the Resonon having slightly lower prediction error for all pigments, except diadinoxanthin, where the Coral-ACTIS was a better predictor (Figure 5). The optimal NoC varied greatly by instrument, with the optimal NoC for all Coral-ACTIS pigments being 1 component, while the NoC for the Resonon predicted pigments was higher and more variable (chlorophyll *a*, *c*2 = 5 components, diadinoxanthin = 3, peridinin = 4, total pigments = 7). The 95% prediction intervals were comparable between the two instruments but slighter higher in the Resonon predicted pigments with a higher NoC (Chlorophyll *a*, c2, total pigments) due to the increased model complexity (Figure 5). The VIP analysis showed that in the Resonon spectra, wavelengths between ~500 and 580 nm were the most important across pigments (VIP > 1.0), but the overall VIP score was high across the majority of wavelengths (~500 – 690 nm, VIP > 0.8; Supplementary Figure S2). In the Coral-ACTIS spectra, the most important wavelengths were slightly longer (~540 – 640 nm, VIP > 1.0) with even higher VIP scores (VIP >1.2) around specific peaks for Chlorophyll *a*, c2 and total pigments and VIP scores were lower outside of this range reflecting the single-component model structure (Supplementary Figure S2).

 doi:10.20944/preprints202605.0114.v1

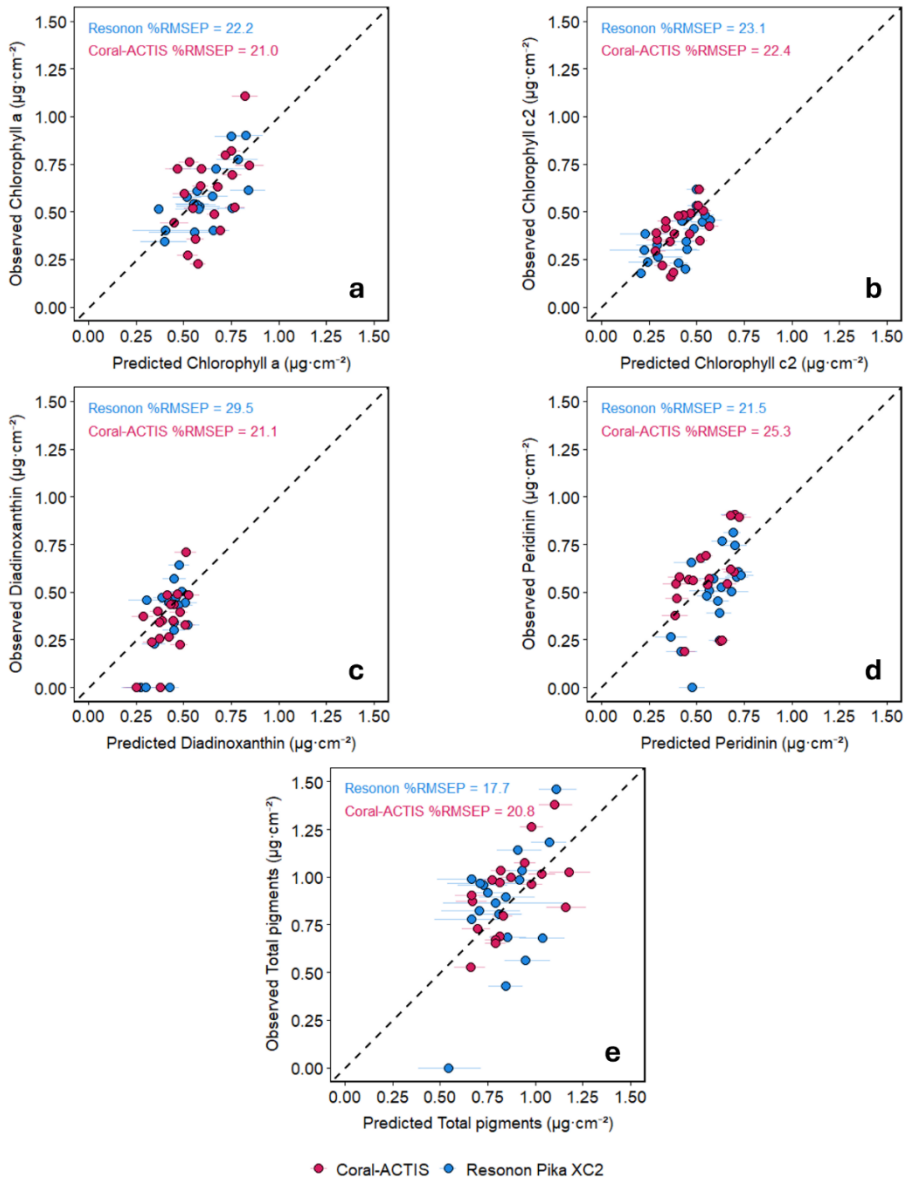

Figure 5. (**a** – **e)** Partial Least Squares Regression (PLSR) predicted pigment concentrations from hyperspectral reflectance data obtained with Coral-ACTIS DIY hyperspectral camera and Resonon Pika XC2 commercial HSI vs observed pigment concentrations (laboratory assayed). Dashed lines represent perfect 1:1 agreement. The optimal number of components (NoC) used for each pigment–sensor combination. Error bars represent 95% bootstrap prediction intervals. Pigment values are cube-root transformed.

Camera Sensitivities and Comparison of Reference Spectra

The spectral sensitivities of the Sony 8 mega-pixel IMX219 image sensor within the Raspberry PI NOIR V2 module of the Coral-ACTIS was determined during the calibration process (Figure 6). The spectral sensitivities and RGB crossover points obtained via the self-calibration process aligned closely with the manufacturer's reference measurements of the sensor (Sony Corporation, 2019). Coral-ACTIS acquired spectra of CFL and Halogen light bulbs were comparable to measurements acquired via the Ocean Optics Flame Series Miniature Spectrometer (Figure 7). The halogen spectra were more similar between the Coral-ACTIS and the spectrometer with a high R^2 of 0.884 and a spectral angle of 10.6°. The CFL spectra peaks were aligned in each HSI instrument but were much broader in the Coral-ACTIS, and the overall shape was less similar to the reference than for the Resonon (Figure 7; $R^2 = 0.478$; spectral angle = 40.2°).

 doi:10.20944/preprints202605.0114.v1

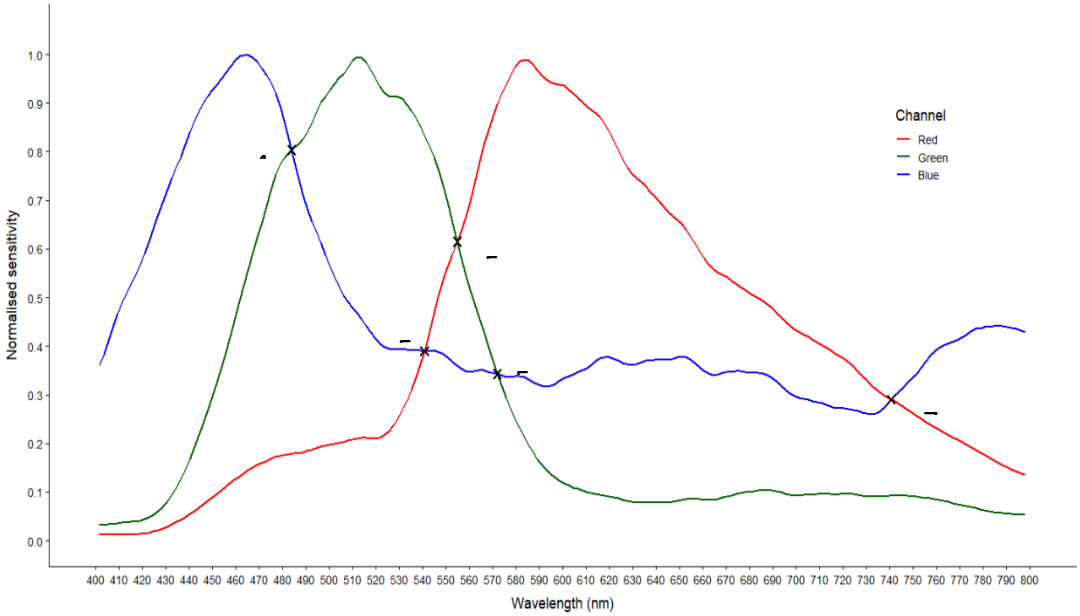

Figure 6. Spectral sensitivities and crossover points of the Coral-ACTIS's RGB channels.

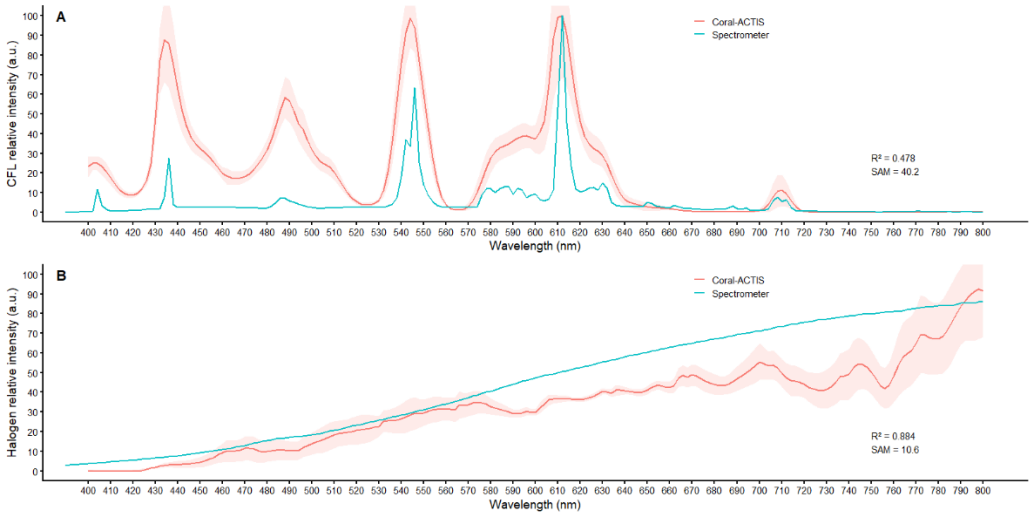

Figure 7. Comparison of mean relative intensity ± SD of (**A**) compact fluorescent lamp (CFL) and (**B**) halogen light reference spectra using measurements taken using the Coral-ACTIS camera and an Ocean Optics Flame Series Miniature Spectrometer. To enable comparison of spectral shape spectrometer units (μW· cm $^{-2}$) and Coral-HSI digital number (DN), values were scaled (0–100, arbitrary units (a.u.)) with zero set using the background dark noise and 100% as the highest peak intensity measured (n = 5 instantaneous spectrometer measurements and Coral-HSI regions of interest per spectra).

Discussion

Coral Reflectance Comparison

Spectral angle mapping (SAM) showed there was a moderate to high amount of similarity between the two HSIs with a mean spectral angle of 0.199 ± 0.067 radians (11.38 ± 3.82°). However, SAM primarily considers the shape of the spectra, rather than their magnitudes (Kruse et al., 1993). SAM is beneficial to compare the Coral-ACTIS with the reference lights or for use in classification tasks where spectral shape is more relevant than potential differences in intensity arising from illumination variability or other effects. However, the moderate to high amount of similarity in the

 doi:10.20944/preprints202605.0114.v1

SAM is not necessarily reflective of the overall similarity between the Coral-ACTIS and commercial HSI, as accurate detection of the spectra magnitude is crucial for detecting changes in bleaching severity (Asner et al., 2024; Holden & LeDrew, 1998). When comparing individual key reflectance wavelengths in the PERMANOVAs, the Coral-ACTIS was only able to detect differences among sampling days, while the commercial HSI found significant temperature effects. The spectral angle values on the first sampling day were also significantly higher compared to those of the following sampling days. Overall, the PERMANOVA and SAM findings show that if the Coral-ACTIS was used in place of the commercial HSI, it would have led to an incorrect interpretation of the bleaching severity observed during this study, but that the Coral-ACTIS may have potential for spectral classification applications.

PLSR and Prediction of Pigments

In the PLSR analysis, the optimal number of components to explain the relationships between the HSIs and the pigments varied by the HSI used. In the Commercial HSI data, 3 – 7 components were optimal depending on the pigment, while for the Coral-ACTIS, all pigments required only 1 component. This was likely due to the flatter spectral response and lack of a clear 680 nm chlorophyll absorption feature in the Coral-ACTIS requiring less components to explain. The Resonon spectra also contained additional variance related to temperature treatment where the Coral-ACTIS did not detect any significant differences as a result of temperature, simplifying the predictor matrix. The VIP scores support this with the Resonon spectra having high VIP scores across the spectra, while the Coral-ACTIS VIP scores were more centred around specific peaks meaning the components were built from a smaller set of wavelengths compared to the Resonon spectra. This result is comparable to Asner et al. (2024), who did not report the optimal NoCs, but also found high VIP scores for all wavelengths relevant to pigment profiles of the coral species measured (420–670 nm; *Montipora capitata* and *Porites compressa*).

The two HSIs were largely similar in their prediction of key pigments with moderate to low error when predicting samples in the validation set (17.7–29.5 %RMSEP). The slightly lower %RMSEP in the Coral-ACTIS was likely caused by its components being built from a smaller set of wavelengths due to the flatter response and less prominent differences between treatments. Hyperspectral reflectance is most often evaluated as a tool for classification of reef habitats or benthic composition into various indices or species (Khaled & Abdelsalam, 2025; Mishra et al., 2007; Watty et al., 2026), and when reflectance is used to predict pigment concentrations, the various statistical and spectra acquisition methodologies make comparison among studies challenging. Hochberg et al. (2025) and Joyce & Phinn (2003) found lower predictive performance ($R^2 < 0.1$) using spectrometers to measure reflectance, but R^2 is highly subject to changes in variance of pigment concentrations, which are known to vary greatly by species and season among corals (Asner et al., 2024; Warner et al., 2002). Asner et al. (2024) conducted a more comparable study using airborne hyperspectral images, in-water spectrometers and analysed the data using PLSR, finding a slightly higher prediction error for Chlorophyll *a* (34.92 %RMSEP) and Chlorophyll *c2* (36.68%, testing set) compared to those in the present study (21.0% to 23.1 %RMSEP, respectively).

Overall, the ability of each HSI device to predict coral pigments was moderate to good compared to previous studies, but insufficient to be considered as a non-invasive alternative to laboratory assays of coral pigments. However, the reflectance at key wavelengths was effective for measuring changes in coral health due to temperature stress when measured with the commercial HSI. These reflectance indices could be used as a more robust alternative to colour measurements obtained with RGB cameras and colour charts (Ferrara et al., 2024; Siebeck et al., 2006) with greater potential for cross-study comparability when using radiometrically-corrected hyperspectral data.

The Coral-ACTIS was unable to detect differences among temperature treatments; this is likely due to its less-precise calibration and correction process compared to the commercial HSI. Reduced dynamic range in the Coral-ACTIS sensor may have limited the range of detectable spectral variation, particularly in the later sampling days where coral in some treatments were highly reflective (Day 52 and 65). Signal attenuation at spectral extremes could have further limited detection of subtle

 doi:10.20944/preprints202605.0114.v1

reflectance differences, a known limitation of the low-cost HSI (Salazar-Vazquez & Mendez-Vazquez, 2020). Furthermore, the accumulation of small shifts in camera and coral position, lighting, and lens focus could contribute to its reduced performance. A future version of the camera's Linux app with built-in reflectance scaling and broader correction methods (rather than the current red, green and blue peak identification) would likely reduce these errors. However, the calibration would require more precise reference lights with known spectra, or a spectrometer to implement, either of which would likely cost more than the Coral-ACTIS itself.

Coral-ACTIS vs Reference Light Spectra

The Coral-ACTIS was better able to reproduce the halogen bulb spectra than the CFL. This was due to the halogen bulb having a much broader spectrum with gradual changes, while the CFL spectrum had high-intensity, narrow peaks. The largest deviation between the two instruments occurred at ~485 nm, where the Coral-ACTIS peak was much larger than the spectra detected by the spectrometer. This was likely due to the spectral sensitivities of the Sony IMX219 sensor. There was considerable overlap and channel crosstalk between the blue and green sensitivities at this specific region. The Bayer filter matrix, the most common filter arrangement across all digital cameras, contains twice as many green pixels as red or blue pixels, which may contribute to artifacts in the spectral reconstruction (Eöllös-Jarošíková et al., 2025; Lukac & Plataniotis, 2005). Bayer interpolation and demosaicing algorithms account for this by using a different weighting for the green pixels, but the quantum efficiency of CMOS (and all silicon-based sensors) often peaks in the same wavelength region where crosstalk with the blue channel and image demosaicing issues may occur (~490 nm; Tucsen, 2025). The absence of a corresponding spectral artefact at ~490 nm in the halogen light source was likely due to the smooth emission curve of the halogen spectra having no narrow features for the crosstalk to interpret and amplify incorrectly. The coral spectra were similarly unaffected, likely again due to smooth transitions in reflectance limiting interpolation issues.

Currently the image demosaicing process is handled by a proprietary algorithm within the Raspberry Pi 4b's Broadcom BCM2711 image signal processor. Images from the Coral-ACTIS could be saved as raw DNGs without demosaicing applied and processed via different algorithms for potentially more accurate colours. Traditional approaches interpolate missing colour values from neighbouring pixels of the same channel, often weighting the interpolation along detected edges to preserve sharpness (Menon & Calvagno, 2011). Newer content-aware learning algorithms analyse the surrounding image structure to adaptively choose interpolation direction and weighting on a per-pixel basis, but are more computationally expensive (Luo & Wang, 2020). Overall, a different demosaicing algorithm may offer a more accurate spectral response but is likely to increase computational load and would require a new imaging processing pipeline for the Coral-ACTIS's control software. The combination of potential factors (channel crosstalk, Bayer filter and CMOS quantum efficiency) makes determining the cause and correcting for spectral irregularities difficult.

 doi:10.20944/preprints202605.0114.v1

Future Coral Spectral Imaging

A future version of the Coral-ACTIS may be able to eliminate a portion of the spectral irregularities by using alternate sensor designs that do not rely on colour filter arrays, such as multi-sensor CCDs, which contain individual sensors for each colour channel and do not require demosaicing, resulting in less colour overlap and better colour accuracy (Ahmad et al., 2019). It is also possible to avoid these issues by using an alternate optical design, such as the Bi-Frost DSLR developed by Teague et al. (2023), which uses a linear variable filter band-scanning design in which only one wavelength of light is projected onto a monochrome sensor at a time (Figure 1). However, LVFs are expensive (USD $2,000 – $7,000) depending on bandwidth range and resolution) and require the use of a translation stage and/or image stitching to reconstruct the images. Other Snapshot HSI designs exist but often rely on computationally-intensive image reconstruction combined with advanced microlenses, metasurfaces, filter arrays, and/or optic-fibre bundles that are not easily replicated using consumer off the shelf components (Monakhova et al., 2020; Podlesnykh et al., 2024; Y. Wang et al., 2019).

Instead of using a hyperspectral approach to measure coral reflectance, monochrome cameras and bandpass filters could be combined to build a low-cost (USD ~$500 – 600) multispectral camera that could avoid the difficult calibration process, Bayer interpolation, image reconstruction and other drawbacks present in CTIS and other hyperspectral camera designs. By selecting bandpass filters specific to wavelengths that are markers for coral health (in the 450 – 710 nm range), the camera could calculate simple reflectance metrics or normalised indices to provide instant assessments of coral health, avoiding longer processing times and interpretation of high-dimensionality waveband data. However, more work is needed to determine the optimal wavebands and resolution across a variety of coral species, and such a multispectral camera would be specific to measuring coral health (pigmentation) indices with less general-use utility.

The high number of wavebands in hyperspectral cameras has greater potential for reef habitat/species classification, mapping and detecting other unique spectral signatures like markers of coral disease (Khaled & Abdelsalam, 2025; Melamed et al., 2025). Additionally, we hypothesize that the Coral-ACTIS and other low-cost HSI are best suited for these tasks where the shape of the spectral response is the primary factor (habitat/species classification and disease detection), whereas in coral bleaching the shape of the reflectance spectra remains more consistent and smaller changes in magnitude occur as coral pigments are lost (Khaled & Abdelsalam, 2025; Melamed et al., 2025; Teague et al., 2022).

Continuing to develop hyperspectral cameras suited for general use also benefits other areas of research. HSIs have seen a recent surge in utilitisation across an endless variety of disciplines ranging from agricultural science, medical analysis, product quality control, counterfeit detection, archaeology, geology and more (Reviewed by Cheng et al., 2025). Continued development of easy-to-use and affordable hyperspectral platforms stands to draw from and feed back into research advances across a diverse range of fields, whereas a multispectral camera designed for a single application lacks this broader development base of end-users.

Conclusion

Overall, the low-cost hyperspectral camera (Coral-ACTIS) produced spectral shapes similar to those of the commercial Resonon Pika XC2 camera in some tests; however, it lacked the ability to detect intensities as precisely as the Pika XC2. Given the large cost difference (USD $201 vs ~USD $70,000) and the development and calibration of the systems, this difference in performance was not unexpected. The Coral-ACTIS had limited ability to consistently detect spectral response magnitude and was unable to detect significant differences among temperature treatments where the commercial HSI did. The current iteration of the Coral-ACTIS is better suited to diagnostic and classification tasks in which spectral shape is the primary discriminating factor rather than the response magnitude but improvements to calibration or sensor design in future versions could overcome these issues. Cost is a significant barrier to the wider adoption of hyperspectral imaging,

 doi:10.20944/preprints202605.0114.v1

and as low-cost HSI designs are refined, easier access to the technology can enhance efforts in coral reef restoration and environmental research more broadly.

Supplementary Materials: The following supporting information can be downloaded at the website of this paper posted on Preprints.org.

Author Contributions: Conor Hendrickson: Conceptualisation, Investigation, Formal analysis, Methodology, Visualisation, Writing - Original Draft, Reviewing and Editing. **Peter Butcherine**: Conceptualisation, Methodology, Writing – Review & Editing. **Daniel P. Harrison**: Supervision, Funding acquisition, Writing – Review & Editing. **Brendan P. Kelaher**: Supervision, Funding acquisition, Conceptualisation, Methodology, Writing – Review & Editing.

Acknowledgments: The authors would like to acknowledge the Traditional Owners of the Bindal and Gumbaynggirr country where this study was conducted and all Traditional Owners of the Great Barrier Reef and its Catchments as First Nations Peoples who hold the hopes, dreams, traditions, and cultures of the Reef. We thank the Reef Restoration and Adaptation Program (RRAP), Peter Marshall and Pauline Graham for their extensive administrative assistance. The Reef Restoration and Adaptation Program is funded by the partnership between the Australian Governments Reef Trust and the Great Barrier Reef Foundation. We thank Matt Salmon, David Hughes, and the research technicians of the National Sea Simulator facility, Australian Institute of Marine Science, for their experimental assistance.

Funding: This work was supported by The Reef Restoration and Adaptation Program (Australia) and Southern Cross University.

Conflicts of Interest: The authors declare that the research was conducted in the absence of any commercial or financial relationships that could be construed as a potential conflict of interest.

Declaration of Competing Interest: The authors declare that they have no known competing financial interests or personal relationships that could have appeared to influence the work reported in this paper.

Data availability: Data will be made available on request.

References

1. Abd-Elrahman, A., Pande-Chhetri, R., & Vallad, G. (2011). Design and development of a multi-purpose low-cost hyperspectral imaging system. *Remote Sensing*, *3*(3), 570–586.
2. Ahmad, A., Kumar, A., Dubey, V., Butola, A., Ahluwalia, B. S., & Mehta, D. S. (2019). Characterization of color cross-talk of CCD detectors and its influence in multispectral quantitative phase imaging. *Optics Express*, *27*(4), 4572–4589. https://doi.org/10.1364/OE.27.004572
3. Anderson, M. J. (2001). A new method for non-parametric multivariate analysis of variance. *Austral Ecology*, *26*(1), 32–46. https://doi.org/10.1111/j.1442-9993.2001.01070.pp.x
4. Asner, G. P., Drury, C., Vaughn, N. R., Hancock, J. R., & Martin, R. E. (2024). Variability in Symbiont Chlorophyll of Hawaiian Corals from Field and Airborne Spectroscopy. *Remote Sensing*, *16*(5), 732. https://doi.org/10.3390/rs16050732
5. Bhargava, A., Sachdeva, A., Sharma, K., Alsharif, M. H., Uthansakul, P., & Uthansakul, M. (2024). Hyperspectral imaging and its applications: A review. *Heliyon*, *10*(12). https://doi.org/10.1016/j.heliyon.2024.e33208
6. Burnett, A. C., Anderson, J., Davidson, K. J., Ely, K. S., Lamour, J., Li, Q., Morrison, B. D., Yang, D., Rogers, A., & Serbin, S. P. (2021). A best-practice guide to predicting plant traits from leaf-level hyperspectral data using partial least squares regression. *Journal of Experimental Botany*, *72*(18), 6175–6189. https://doi.org/10.1093/jxb/erab295
7. Butcherine, P., Fiori, A., Ellis, S. L., Hendrickson, C. A., & Harrison, D. P. (2026). *Shading Acropora kenti during doldrum-like conditions can reduce mortality risk during high-thermal stress events*. In Review. https://doi.org/10.21203/rs.3.rs-8633876/v1

 doi:10.20944/preprints202605.0114.v1

8. Carrascal, L. M., Galván, I., & Gordo, O. (2009). Partial least squares regression as an alternative to current regression methods used in ecology. *Oikos*, *118*(5), 681–690. https://doi.org/10.1111/j.1600-0706.2008.16881.x
9. Cheng, M.-F., Mukundan, A., Karmakar, R., Valappil, M. A. E., Jouhar, J., & Wang, H.-C. (2025). Modern Trends and Recent Applications of Hyperspectral Imaging: A Review. *Technologies*, *13*(5), 170. https://doi.org/10.3390/technologies13050170
10. Chennu, A., Färber, P., De'ath, G., de Beer, D., & Fabricius, K. E. (2017). A diver-operated hyperspectral imaging and topographic surveying system for automated mapping of benthic habitats. *Scientific Reports*, *7*(1), 7122. https://doi.org/10.1038/s41598-017-07337-y
11. Eöllös-Jarošíková, K., Guerra-Yánez, C., Zvánovec, S., & Komanec, M. (2025). Fog resilient optical camera communication using wavelength division multiplexing. *Optics Express*, *33*(19), 39426–39437. https://doi.org/10.1364/OE.570269
12. Ferrara, E. F., Bauer, L., Puntin, G., Bautz, F., Celayir, S., Do, M.-S., Eck, F., Heider, M., Wissel, P., Arnold, A., Wilke, T., Reichert, J., & Ziegler, M. (2024). *RGB color indices as proxy for symbiont cell density and chlorophyll content during coral bleaching* (p. 2024.12.20.629333). bioRxiv. https://doi.org/10.1101/2024.12.20.629333
13. Hochberg, E. J., Atkinson, M. J., Apprill, A., & Andréfouët, S. (2004). Spectral reflectance of coral. *Coral Reefs*, *23*(1), 84–95. https://doi.org/10.1007/s00338-003-0350-1
14. Hochberg, E. J., Ducret, H., & Dierssen, H. M. (2025). Revised empirical models for estimating coral pigment concentrations from optical reflectance spectra. *Applied Optics*, *64*(35), 10603–10610. https://doi.org/10.1364/AO.578421
15. Holden, H., & LeDrew, E. (1998). Spectral Discrimination of Healthy and Non-Healthy Corals Based on Cluster Analysis, Principal Components Analysis, and Derivative Spectroscopy. *Remote Sensing of Environment*, *65*(2), 217–224. https://doi.org/10.1016/S0034-4257(98)00029-7
16. Joyce, K. E., & Phinn, S. R. (2003). Hyperspectral analysis of chlorophyll content and photosynthetic capacity of coral reef substrates. *Limnology and Oceanography*, *48*(1part2), 489–496.
17. Khaled, M. A., & Abdelsalam, A. A. (2025). Discrimination of some red sea coral reef species based on hyperspectral signature field data. *Scientific African*, *28*, e02696. https://doi.org/10.1016/j.sciaf.2025.e02696
18. Kruse, F. A., Lefkoff, A. B., Boardman, J. W., Heidebrecht, K. B., Shapiro, A. T., Barloon, P. J., & Goetz, A. F. H. (1993). The spectral image processing system (SIPS)—Interactive visualization and analysis of imaging spectrometer data. *Remote Sensing of Environment, Airbone Imaging Spectrometry*, *44*(2), 145–163. https://doi.org/10.1016/0034-4257(93)90013-N
19. Lukac, R., & Plataniotis, K. N. (2005). Color filter arrays: Design and performance analysis. *IEEE Transactions on Consumer Electronics*, *51*(4), 1260–1267.
20. Luo, J., & Wang, J. (2020). Image Demosaicing Based on Generative Adversarial Network. *Mathematical Problems in Engineering*, *2020*(1), 7367608. https://doi.org/10.1155/2020/7367608
21. Melamed, M. B., Martin, R. E., Allen, M., & Asner, G. P. (2025). Reflections: Spectral Investigation of Black Band Disease in Hawaiian Corals. *Remote Sensing*, *17*(18), 3241. https://doi.org/10.3390/rs17183241
22. Menon, D., & Calvagno, G. (2011). Color image demosaicking: An overview. *Signal Processing: Image Communication*, *26*(8), 518–533. https://doi.org/10.1016/j.image.2011.04.003
23. Mevik, B.-H., & Wehrens, R. (2007). The pls package: Principal component and partial least squares regression in R. *Journal of Statistical Software*, *18*, 1–23.
24. Mishra, D. R., Narumalani, S., Rundquist, D., Lawson, M., & Perk, R. (2007). Enhancing the detection and classification of coral reef and associated benthic habitats: A hyperspectral remote sensing approach. *Journal of Geophysical Research: Oceans*, *112*(C8). https://doi.org/10.1029/2006JC003892
25. Monakhova, K., Yanny, K., Aggarwal, N., & Waller, L. (2020). Spectral DiffuserCam: Lensless snapshot hyperspectral imaging with a spectral filter array. *Optica*, *7*(10), 1298–1307. https://doi.org/10.1364/OPTICA.397214
26. Montes-Herrera, J. C., Cimoli, E., Cummings, V., Hill, N., Lucieer, A., & Lucieer, V. (2021). Underwater hyperspectral imaging (UHI): A review of systems and applications for proximal seafloor ecosystem studies. *Remote Sensing*, *13*(17), 3451.

 doi:10.20944/preprints202605.0114.v1

27. Podlesnykh, I., Kovalev, M., & Platonov, P. (2024). Towards the Future of Ubiquitous Hyperspectral Imaging: Innovations in Sensor Configurations and Cost Reduction for Widespread Applicability. *Technologies*, *12*(11), 221. https://doi.org/10.3390/technologies12110221
28. Polder, G., & Gowen, A. (2021). The hype in spectral imaging. *Spectroscopy Europe*. https://library.wur.nl/WebQuery/wurpubs/fulltext/574548
29. Rashid, A. R., & Chennu, A. (2020). A Trillion Coral Reef Colors: Deeply Annotated Underwater Hyperspectral Images for Automated Classification and Habitat Mapping. *Data*, *5*(1), Article 1. https://doi.org/10.3390/data5010019
30. Richards, L. S., Siems, S. T., Huang, Y., Zhao, W., Harrison, D. P., Manton, M. J., & Reeder, M. J. (2024). The meteorological drivers of mass coral bleaching on the central Great Barrier Reef during the 2022 La Niña. *Scientific Reports*, *14*(1), 1–17.
31. Salazar-Vazquez, J., & Mendez-Vazquez, A. (2020). A plug-and-play Hyperspectral Imaging Sensor using low-cost equipment. *HardwareX*, *7*, e00087. https://doi.org/10.1016/j.ohx.2019.e00087
32. Savitzky, Abraham., & Golay, M. J. E. (1964). Smoothing and Differentiation of Data by Simplified Least Squares Procedures. *Analytical Chemistry*, *36*(8), 1627–1639. https://doi.org/10.1021/ac60214a047
33. Siebeck, U. E., Marshall, N. J., Klüter, A., & Hoegh-Guldberg, O. (2006). Monitoring coral bleaching using a colour reference card. *Coral Reefs*, *25*(3), 453–460. https://doi.org/10.1007/s00338-006-0123-8
34. Sony Semiconductor Solutions Corporation. (2019). *IMX219PQ CMOS Image Sensor Datasheet*. Available online: https://www.opensourceinstruments.com/Electronics/Data/IMX219PQ.pdf
35. Stuart, M. B., McGonigle, A. J. S., Davies, M., Hobbs, M. J., Boone, N. A., Stanger, L. R., Zhu, C., Pering, T. D., & Willmott, J. R. (2021). Low-Cost Hyperspectral Imaging with A Smartphone. *Journal of Imaging*, *7*(8), Article 8. https://doi.org/10.3390/jimaging7080136
36. Teague, J., Megson-Smith, D. A., Allen, M. J., Day, J. C., & Scott, T. B. (2021). *A Review of Optical Techniques for Coral Monitoring & Introducing Low-Cost Hyperspectral Imaging*.
37. Teague, J., Willans, J., Megson-Smith, D. A., Day, J. C. C., Allen, M. J., & Scott, T. B. (2022). Using Colour as a Marker for Coral 'Health': A Study on Hyperspectral Reflectance and Fluorescence Imaging of Thermally Induced Coral Bleaching. *Oceans*, *3*(4), Article 4. https://doi.org/10.3390/oceans3040036
38. Thrane, J.-E., Kyle, M., Striebel, M., Haande, S., Grung, M., Rohrlack, T., & Andersen, T. (2015). Spectrophotometric Analysis of Pigments: A Critical Assessment of a High-Throughput Method for Analysis of Algal Pigment Mixtures by Spectral Deconvolution. *PLOS ONE*, *10*(9), e0137645. https://doi.org/10.1371/journal.pone.0137645
39. Tucsen. (2025, September 30). *Quantum Efficiency in Scientific Cameras: A Beginner's Guide*. Tucsen. https://www.tucsen.com/learning/quantum-efficiency-in-scientific-cameras/
40. Veal, C. J., Carmi, M., Fine, M., & Hoegh-Guldberg, O. (2010). Increasing the accuracy of surface area estimation using single wax dipping of coral fragments. *Coral Reefs*, *29*, 893–897.
41. Wang, L., Jin, J., Song, Z., Wang, J., Zhang, L., Rehman, T. U., Ma, D., Carpenter, N. R., & Tuinstra, M. R. (2020). LeafSpec: An accurate and portable hyperspectral corn leaf imager. *Computers and Electronics in Agriculture*, *169*, 105209. https://doi.org/10.1016/j.compag.2019.105209
42. Wang, Y., Pawlowski, M. E., Cheng, S., Dwight, J. G., Stoian, R. I., Lu, J., Alexander, D., & Tkaczyk, T. S. (2019). Light-guide snapshot imaging spectrometer for remote sensing applications. *Optics Express*, *27*(11), 15701–15725. https://doi.org/10.1364/OE.27.015701
43. Warner, M., Chilcoat, G., McFarland, F., & Fitt, W. (2002). Seasonal fluctuations in the photosynthetic capacity of photosystem II in symbiotic dinoflagellates in the Caribbean reef-building coral Montastraea. *Marine Biology*, *141*, 31–38.
44. Watty, K., Schoepf, V., Johnson, K. W., Littke, S., & van der Zande, R. M. (2026). Using reflectance to measure chlorophyll a in corals: Calibration and implications of skeletal optical properties. *Coral Reefs*. https://doi.org/10.1007/s00338-026-02831-0
45. Zeng, K., Xu, Z., Yang, Y., Liu, Y., Zhao, H., Zhang, Y., Xie, B., Zhou, W., Li, C., & Cao, W. (2022). In situ hyperspectral characteristics and the discriminative ability of remote sensing to coral species in the South China Sea. *GIScience & Remote Sensing*, *59*(1), 272–294.

 doi:10.20944/preprints202605.0114.v1